Int. J. Heat Mass Transfer. Vol. 35, No. 8, pp. 1865–1880, 1992
Printed in Great Britain

0017–9310/92 $5.00 + 0.00

Channel height effects on forced-convection boiling and critical heat flux from a linear array of discrete heat sources

T. C. WILLINGHAM and I. MUDAWAR

Boiling and Two-Phase Flow Laboratory, School of Mechanical Engineering, Purdue University, West Lafayette, IN 47907, U.S.A.

(*Received* 9 *July* 1991 *and in final form* 22 *August* 1991)

Abstract—Due to the lack of understanding in the literature of channel height effects on forced-convection boiling and critical heat flux (CHF) in rectangular channels, experiments were performed with FC-72 at 1.36 bar for channel heights of 2, 5, and 10 mm. Boiling heat transfer from a linear array of nine discrete heat sources simulating microelectronic chips was investigated for velocity and liquid subcooling ranges of 13–400 cm s^{-1} and 3–36°C, respectively. Unique to these experiments was the concentration of heat flux on a fraction of the channel perimeter corresponding to the width of the chip, with unheated fluid flowing on either side of the chips. Flow visualization in the 2 mm channel revealed that bubbles in near-saturated flow spanned the entire width of the channel, and increases in velocity and/or subcooling reduced the lateral spread of the bubble layer; on the other hand, bubbles in the 5 and 10 mm channels were primarily confined to the area just above the chips. Using the drift-flux model, an analysis for determining the void fraction in subcooled boiling was developed. Experimental data supported by void fraction predictions and flow visualization suggest the existence of an optimal channel height for which forced-convection CHF is a maximum. For equal flow velocities, maximum CHF values in the present study were obtained with the 5 mm channel.

1. INTRODUCTION

IN THE PAST, heat transfer from electronic circuitry has been achieved through the mixed or forced convection of air; however, the extremely high heat fluxes projected for future microelectronic chips, as well as the increased packaging densities of multi-chip modules, require new and innovative schemes for the cooling of electronic systems [1]. One such alternative is direct immersion cooling, which features an intimate contact between the electronic circuitry and some inert, dielectric liquid. The thermal conductivities of these liquids are much larger than that of air, and this greatly enhances their ability to cool the electronics. In addition, because of the typically low boiling points possessed by some direct immersion coolants, heat transfer from the circuitry can be further ameliorated through nucleate boiling on the chip surface.

Due to the combined effects of bubble agitation at the heated surface, high-frequency vapor–liquid exchange and evaporation, boiling is a very effective mode of heat transfer; consequently, the sudden, drastic elevation in the convection coefficient at the incipience of nucleate boiling generally produces a drop in the temperature of the heated surface. As the heat flux from the surface is increased, nucleate boiling heat transfer continues until critical heat flux (CHF) is attained, at which time there is a transition to film boiling. Many researchers have shown through flow visualization that CHF is induced by conditions leading to the development of a vapor blanket over the heated surface [2–5]. This vapor blanket hinders bulk liquid from replenishing the evaporating liquid at the heated surface, promoting an eventual dryout of the surface. Following dryout, conduction and radiation through the vapor blanket become the dominant modes of heat transfer and, consequently, the temperature of the heated surface rapidly escalates. Ergo, both the understanding of CHF and the ability to predict its occurrence have become of paramount importance to designers of direct immersion applications.

A linear array of discrete heat sources serves as a good model for the analysis of heat transfer from microelectronic chips on a circuit board. Furthermore, flowing coolant across the heat sources transforms the model into a direct immersion application for the cooling of a multi-chip module. It is well known that increases in velocity and/or subcooling of the fluid would expand the nucleate boiling region and delay CHF for such a system [5–9]; however, little has been reported on the effect of size of the flow passage on forced-convection boiling and CHF.

Several researchers, in the interest of nuclear engineering, have investigated the effect of narrow gap spacing on CHF for flow in an annulus. Gambill [10] developed a correlation that worked well for subcooled CHF data from many other studies for gap thicknesses in excess of 2 mm. For thicknesses below 2 mm, the correlation tremendously over-predicted CHF, and Gambill suggested that a diameter effect

NOMENCLATURE

A	flow area in channel normal to flow direction
C_0	flow distribution parameter
c_p	specific heat at constant pressure
g	acceleration due to gravity
H	channel height (2, 5, or 10 mm)
h_{fg}	latent heat of vaporization
P_h	heated perimeter of channel, equal to width of heat source (10 mm)
q''	wall heat flux
q''_m	critical heat flux
T	temperature
T^+	nondimensional temperature defined in equation (7)
ΔT_{sat}	wall superheat, $T_w - T_{sat}$
ΔT_{sub}	degree of liquid subcooling, $T_{sat} - T_{f,cl}$
ΔT_w	temperature gradient between chip and liquid, $T_w - T_{f,cl}$
U	mean inlet liquid velocity
$\overline{u_{gj}}$	weighted mean vapor drift velocity
W	mass flow rate
x	mass vapor quality, W_g/W
Z^+	nondimensional axial coordinate defined in equation (8)
z	axial coordinate.

Greek symbols

$\langle\alpha\rangle$	area weighted average of void fraction
ρ	density
σ	surface tension.

Subscripts

0,cl	point of net vapor generation, Chip 1
e	point at which $T_f = T_{sat}$, assuming thermodynamic equilibrium
f	liquid
g	vapor
m	maximum (critical heat flux)
sat	saturated
sub	subcooled
w	mean chip surface condition.

on CHF exists when the gap thickness decreases to the order of bubble dimensions. Using subcooled water and annulus gap thicknesses of 0.5 and 4 mm, Tolubinskiy *et al.* [11] observed CHF to decrease with decreasing gap spacing for a given velocity. According to Tolubinskiy *et al.*, the reduction in CHF was due to an abatement of flow turbulence and subsequent transverse fluctuations due to the reduction of flow cross-section. Hung and Yao [12] observed CHF to decrease with decreasing gap spacing for Freon-113 and annulus gap thicknesses of 0.32, 0.80, and 2.58 mm. Though there was not a tremendous drop in CHF corresponding to a gap reduction from 2.58 to 0.80 mm, a further decrease in the gap thickness to 0.32 mm considerably lowered CHF. Along with the decrease in CHF, Hung and Yao also noticed increased bubble deformation and coalescence as the gap spacing was reduced. Similarly, other researchers have found CHF to be fairly independent of gap size for thicknesses in excess of a critical dimension, while thicknesses below that dimension drastically reduced CHF [13–15]. This so-called critical dimension varied from study to study depending upon the geometry of the system and the experimental conditions.

The present study features forced-convection boiling and CHF data obtained for a linear array of simulated microelectronic chips in a rectangular flow channel. Unlike previous narrow-gap studies, heat flux in the present study was confined to a fraction of the channel perimeter corresponding to the width of the chips, with unheated fluid flowing on either side of the chips. Experiments were performed with FC-72 at 1.36 bar for channel heights of 2, 5, and 10 mm; the experiments were terminated after CHF was attained on each of the nine chips. Due to the lack of understanding of channel height effects on forced-convection boiling and CHF in rectangular channels, the objective of this study was two-fold: (i) to examine the effects of the three different channel heights on the boiling performance of all chips and (ii) to evaluate the effectiveness of the unheated fluid near the side walls in delaying CHF on the chips.

2. EXPERIMENTAL METHODS

Experimental facility

In order to provide coolant flow across the array of nine simulated microelectronic chips, an experimental flow loop was constructed as shown in Fig. 1. Due to the lack of flow control for the magnetically coupled, centrifugal pump, the flow loop also included a bypass line for variation of the fluid velocity in the test section. Two turbine flow meters were used to measure the flow rate within the test section—one for flow rates below 7.6×10^{-5} m^3 s^{-1} and the other for the larger flow rates (only one flow meter is shown in Fig. 1). The degree of liquid subcooling was achieved through the action of two flat plate heat exchangers, with one connected to a constant temperature bath for fine tuning of the liquid temperature just upstream of the test section. The two-phase mixture engendered in the test section was condensed by water-cooled coils in the condenser/reservoir. Pressure in the system was maintained by regulating the energy input to the immersion heater in the pressurization/expansion tank.

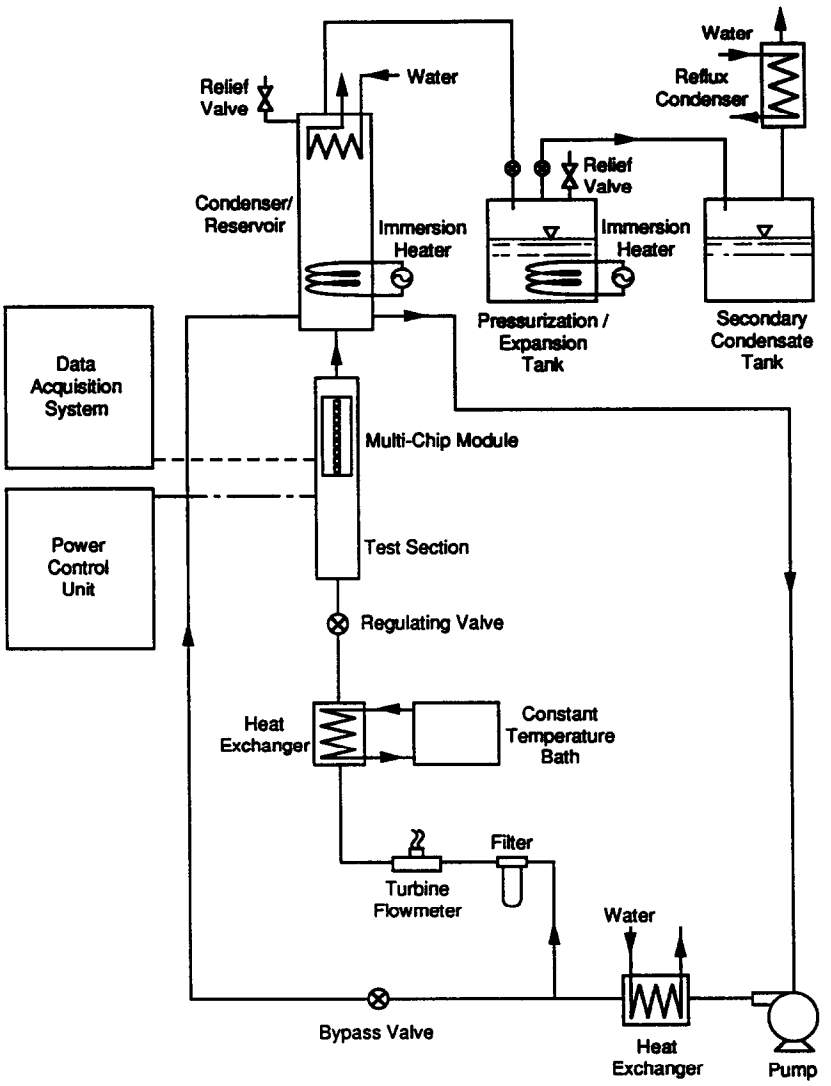

FIG. 1. Experimental flow loop.

The test section was comprised of the rectangular flow channel and the multi-chip module, as shown by the isometric representation in Fig. 2. Though the majority of the flow channel was constructed from G-10 fiberglass insulation, the multi-chip module was machined from high-temperature G-7 fiberglass. In actuality, the module was an entity separate from the channel, and this allowed it to be easily removed from the channel in order to access the chips. The module also formed part of the channel wall in which the chips were mounted, whereas the Lexan window formed the top of the channel and determined the channel height. Three different window sizes rendered channel heights of 2, 5, and 10 mm; the channel width was 20 mm, twice the chip width. For each channel height, one Lexan window was instrumented with pressure and temperature taps to allow local fluid measurements above the chips; the other Lexan window for the same height was clear and permitted flow visualization of the boiling phenomena.

The multi-chip module was positioned in the test section such that the distance between the channel inlet and the most upstream chip was 0.508 m. The most upstream chip in the array was referred to as Chip 1; subsequently, chips farther downstream were assigned progressively higher integers such that the most downstream chip was referred to as Chip 9. Each of the nine simulated microelectronic chips was machined from oxygen-free copper. The square surface of the chip in contact with the coolant had dimensions of 10 mm × 10 mm. A thick-film resistive heater with similar surface area was soldered to the underside of the chip. The nine chips were electrically configured in parallel, and uniform power dissipation for all chips was ensured by adjusting a variable resistor in-line with each chip to account for the variation in actual resistance of the individual resistive heaters. The approximate resistance of each heater was 90 Ω.

Each chip was instrumented with three Chromel–Alumel thermocouples that were embedded along the

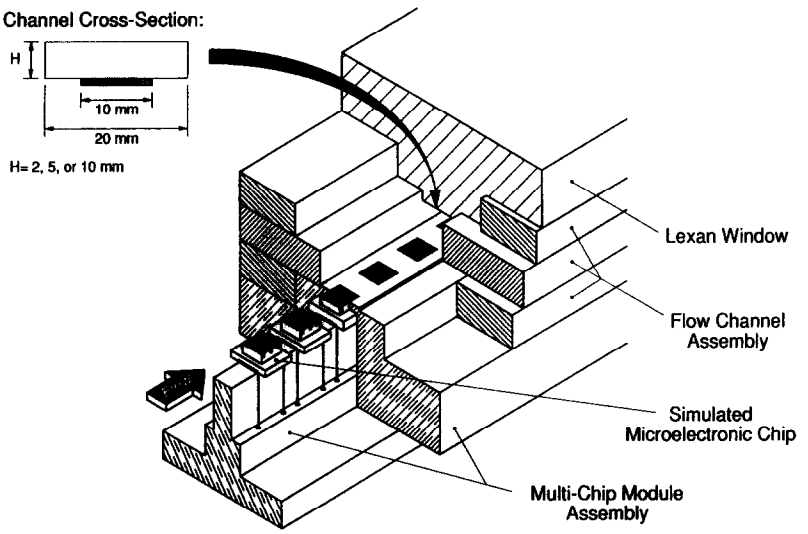

FIG. 2. Test section construction.

chip centerline in the flow direction at a depth of 0.813 mm beneath the chip surface. One thermocouple was centered in the chip, while the other two were located 4.29 mm on either side of this center thermocouple. During experimentation, the thermocouple temperatures were corrected by a one-dimensional heat conduction model to calculate the true chip surface temperature.

Operating procedure

Vapor-blasting of the chip surfaces and deaeration of the fluid both served to create a uniformity in the experimental conditions. In preparation for the study, the chips were cleaned with a vapor blast of fine silica particulates entrained in water flow; the average size of these particulates was 10 μm. Each day of experimentation was commenced with deaeration of the fluid. This was accomplished by raising the fluid temperature to saturation and allowing the air/vapor mixture to enter the condensate tank shown in Fig. 1. A reflux condenser connected to this tank permitted the air to escape to the ambient while the vapor condensed and dripped back into the tank. Upon completion of the deaeration procedure, the valve to the condensate tank was closed.

The operation of a Keithley series 500 data acquisition system was directed by a Compaq microcomputer to obtain the following measurements: three temperatures for each chip, fluid temperature above Chip 1, absolute pressure at Chip 1, differential pressure between the most upstream and downstream chips, frequency of the turbine flow meter, the voltage across the chips, and the individual current through each chip. The pressure at Chip 1 was maintained at 1.36 bar, and this pressure was used in conjunction with the fluid temperature above Chip 1 to determine the inlet subcooling. The saturation temperature for all chips was referenced with respect to the pressure at Chip 1. During an experiment, the power dissipated by the thick-film resistive heater of each chip was incrementally increased, and data points were taken once steady-state conditions were achieved. Steady-state was assumed when 20 data samples for each of the chip temperatures taken over a 20 s period had a standard deviation of less than 0.10°C.

Experimental error

Experimental uncertainties resulted from errors in the various instruments used in the measurements. The maximum error associated with each thermocouple reading was estimated to be less than 0.2°C. Watt and voltage meters with known error bounds were used to calibrate the current and voltage transducers, and the error in measuring the power dissipated by the thick-film resistive heaters was calculated to be a maximum of 0.5%. A two-dimensional finite-difference analysis was performed on the test section to determine the amount of energy dissipated by the resistive heater that was not convected away from the chip by nucleate boiling at the chip surface. An upper limit of the heat loss was then calculated by accounting for the additional surface area on the actual chip and by assuming negligible contact resistances between the copper block and fiberglass insulation. The largest heat loss was determined to be 3%. Combined with the error associated with the electrical power measurement, it was estimated that the maximum uncertainty in heat flux measurement was less than 3.5%.

Calibration accuracies associated with the turbine flow meters for small and large flow velocities were both $\pm 0.05\%$; repeatability for the small and large flow velocities were $\pm 0.1\%$ and $\pm 0.05\%$, respectively. The error associated with the pressure transducer readings was ± 0.0103 bar.

3. RESULTS AND DISCUSSION

The effects of three different channel heights (2, 5, and 10 mm) on forced-convection boiling and CHF were investigated for a linear array of nine simulated microelectronic chips. Experiments were performed with FC-72 at 1.36 bar, while the velocity and subcooling of the coolant were varied from 13 to 400 cm s^{-1} and 3 to 36°C, respectively. The pressure and fluid temperature corresponding to pure liquid at the most upstream chip in the array are two parameters that can easily be measured and/or utilized by designers of electronic cooling schemes. Hence, the saturation temperature and degree of liquid subcooling for all chips in the present study were referenced with respect to the pressure at Chip 1, the most upstream chip. Similarities and differences were observed in the boiling data for different channels and will be discussed in this section.

The boiling curve

There were some general trends observed in the boiling data that appeared to be independent of the channel height. Figures 3(a), (b), and (c) compare the boiling curves for channel heights of 10, 5, and 2 mm, respectively, for Chips 1, 4, and 9 with near-saturated flow at an inlet velocity of 50 cm s^{-1}. The data plotted in Fig. 3 are representative of the fact that for all channels, Chip 9 was generally the first to experience nucleate boiling, and upstream chips followed Chip 9 to boiling incipience in a fairly monotonic succession. Due to its early transition from single- to two-phase heat transfer, Chip 9 experienced the smallest incipience temperature drop of all chips. As the chips progressively reached nucleate boiling, the degree of incipience temperature drop increased such that Chip 1 consistently experienced the largest temperature drop. Figure 3 also reveals that both the shape and slope of the nucleate boiling curve remained the same regardless of the decrease in channel height.

There were also some noticeable differences in the boiling data which seemed to be engendered by the variation in channel height. Throughout the present study, the incipience temperature drops in the 5 and 10 mm channels were similar. However, temperature drops in the 2 mm channel were consistently larger than those observed for the corresponding chips in the other two channels. For all experiments, the surface temperatures of the chips decreased in the flow direction, but this stream-wise decrease grew with reduction in channel height. In Fig. 3(c), the larger stream-wise decrease in surface temperature for the smallest channel is illustrated by a spreading out of the boiling curves for Chips 1, 4, and 9 and is a result of the pressure drop in the channel. For a given inlet velocity, decreasing the channel height results in a larger pressure drop which, subsequently, produces a larger stream-wise decrease in saturation temperature, especially for high flow velocities corresponding to large pressure drops. Furthermore, a lower saturation

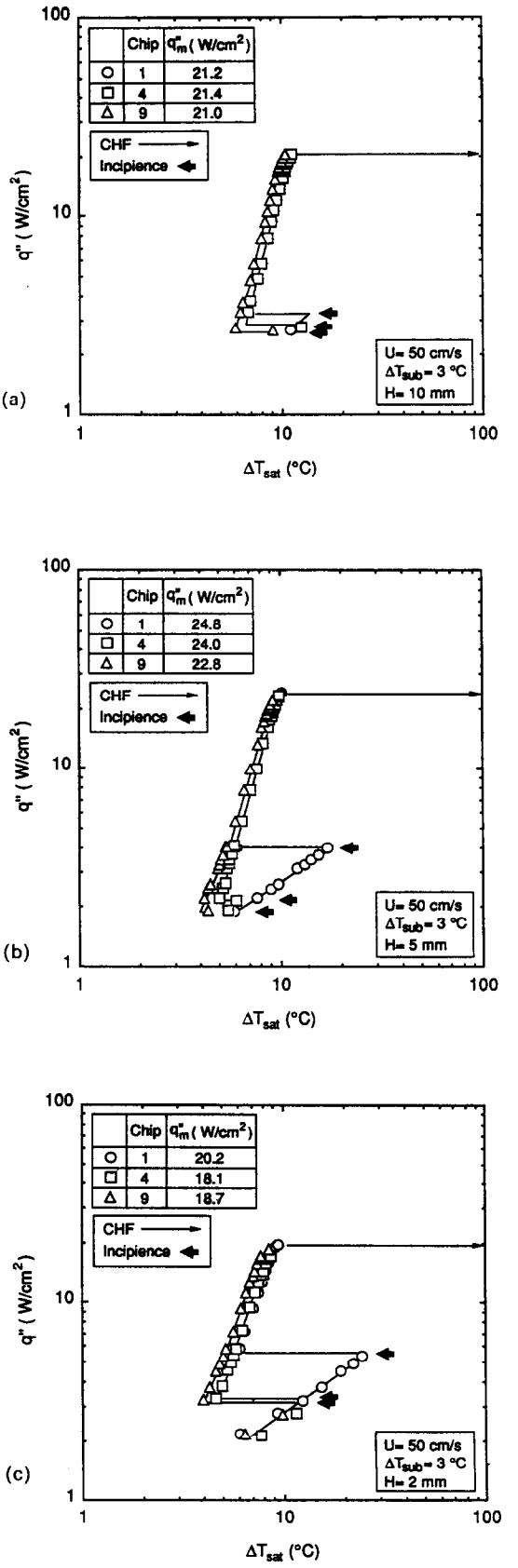

FIG. 3. Boiling curves for Chips 1, 4, and 9 for near-saturated flow at an inlet velocity of 50 cm s^{-1} and channel heights of 10 mm (a), 5 mm (b), and 2 mm (c).

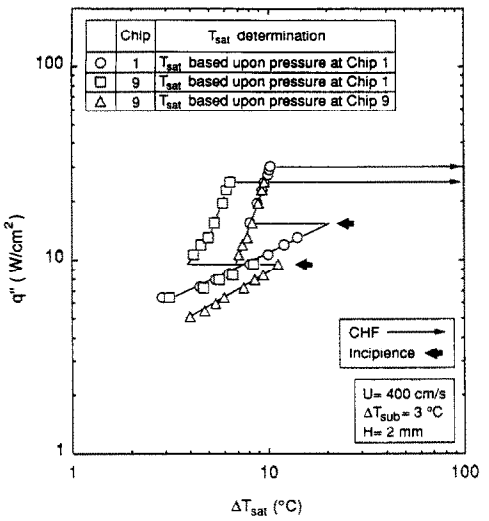

FIG. 4. Effect of pressure drop on boiling curve for 2 mm channel with near-saturated flow and an inlet velocity of 400 cm s^{-1}.

temperature for downstream fluid requires a lower surface temperature for downstream chips to maintain nucleate boiling; however, since the saturation temperature for the entire multi-chip array is referenced with respect to the pressure at Chip 1, the lower surface temperature for Chip 9 causes the nucleate boiling curve to shift to the left. This leftward shift in the boiling curve was most commonly observed in the 2 mm channel for near-saturated flow at a velocity of 400 cm s^{-1}, conditions for which the pressure drop was measured to be a maximum (0.144 bar). In addition to boiling curves for Chips 1 and 9 in these conditions, Fig. 4 shows the boiling curve for Chip 9 when ΔT_{sat} is corrected to account for the stream-wise decrease in saturation temperature (which equalled 3.33°C for the 1.44 bar pressure drop). The corrected boiling data for Chip 9 fall on top of the boiling curve for Chip 1. These data, along with those represented in Figs. 3(a) and (b), demonstrate that all chips in the array had equal fully developed nucleate boiling convection coefficients.

The general effects of channel height on the boiling curve just described were also observed at larger velocities and higher subcoolings than those represented in Fig. 3. The boiling curves for Chips 1, 4, and 9 with highly subcooled flow at an inlet velocity of 400 cm s^{-1} are compared in Figs. 5(a), (b), and (c) for the three channels (10, 5, and 2 mm, respectively). Note that the abscissa in Fig. 5 features the difference between the chip surface temperature and the fluid temperature at Chip 1 (ΔT_w) rather than the wall superheat (ΔT_{sat}). Regardless of channel height, both incipience and CHF were delayed to higher heat fluxes for all chips with increases in velocity and/or subcooling.

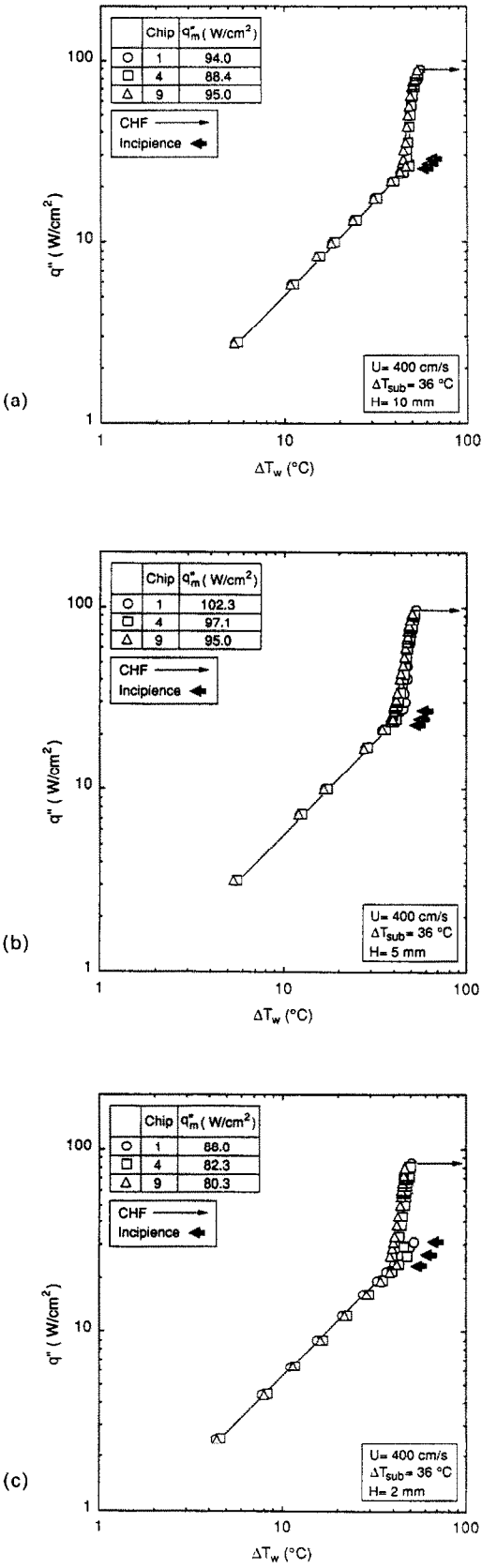

FIG. 5. Boiling curves for Chips 1, 4, and 9 for highly subcooled flow at an inlet velocity of 400 cm s^{-1} and channel heights of 10 mm (a), 5 mm (b), and 2 mm (c).

Flow visualization

Another effect of channel height on the boiling phenomena was observed through flow visualization in the three channels. For flow at 3°C subcooling and 50 cm s^{-1}, Figs. 6(a), (b), and (c) show the bubble populations in the flow above Chips 1 and 9 in the 10, 5, and 2 mm channels, respectively. The photographs were obtained at a chip heat flux of 15 W cm^{-2} and represent fully developed nucleate boiling on the chip surface. Although boiling on Chip 1 appeared almost identical in each of the three channels, there was a marked difference in the appearance of bubbles in the flow above Chip 9 for each channel. In general, bubbles in the 10 mm channel appeared to remain in an area just above the chips without any significant migration towards the side walls of the channel, and only by the time the flow had reached Chip 9 had some of the bubbles reached the top wall of the channel. The 5 mm channel seemed to produce a slightly larger void fraction combined with a little bubble migration

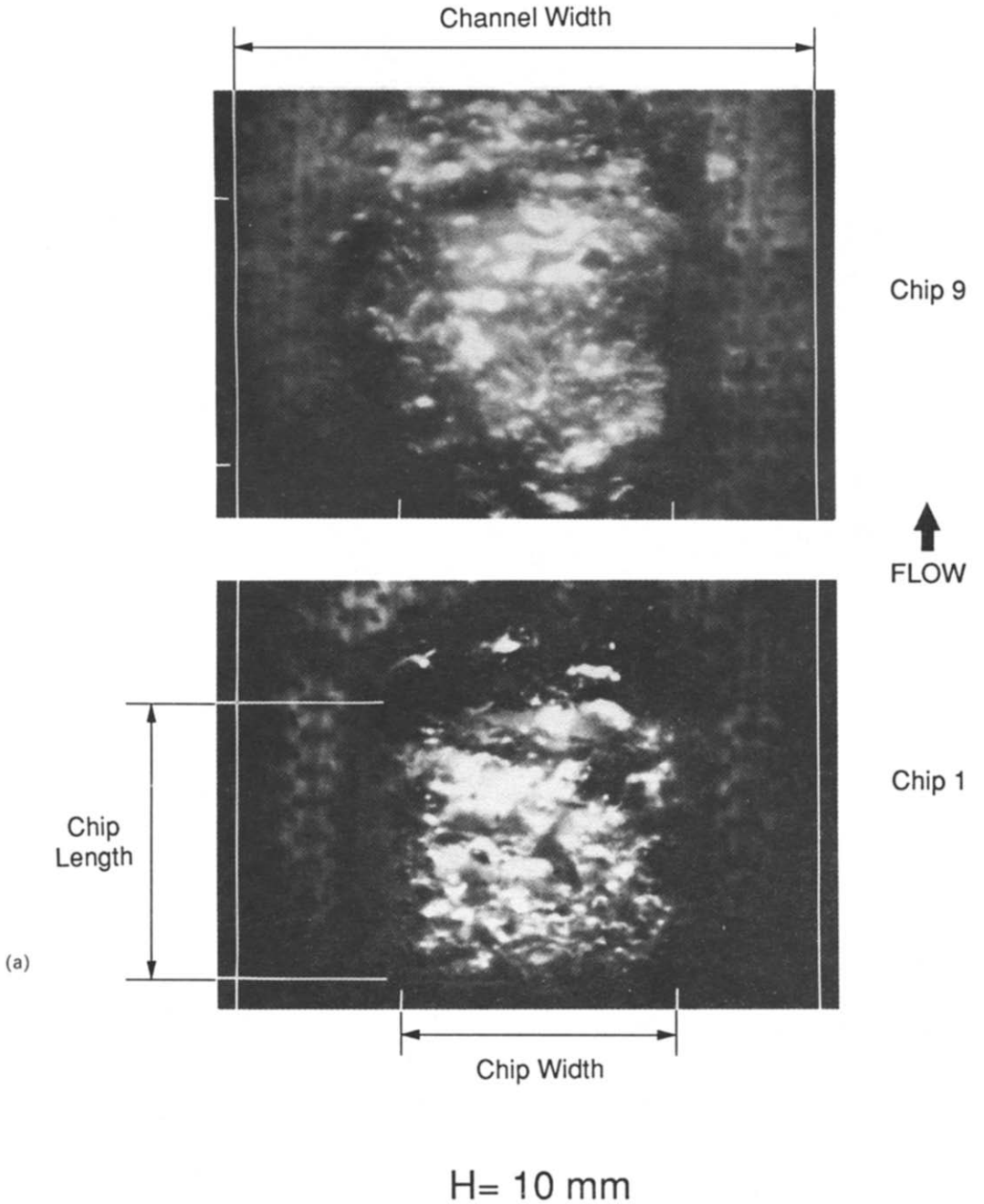

FIG. 6. Photographs of near-saturated flow above Chips 1 and 9 for an inlet velocity of 50 cm s^{-1} and channel heights of 10 mm (a), 5 mm (b), and 2 mm (c).

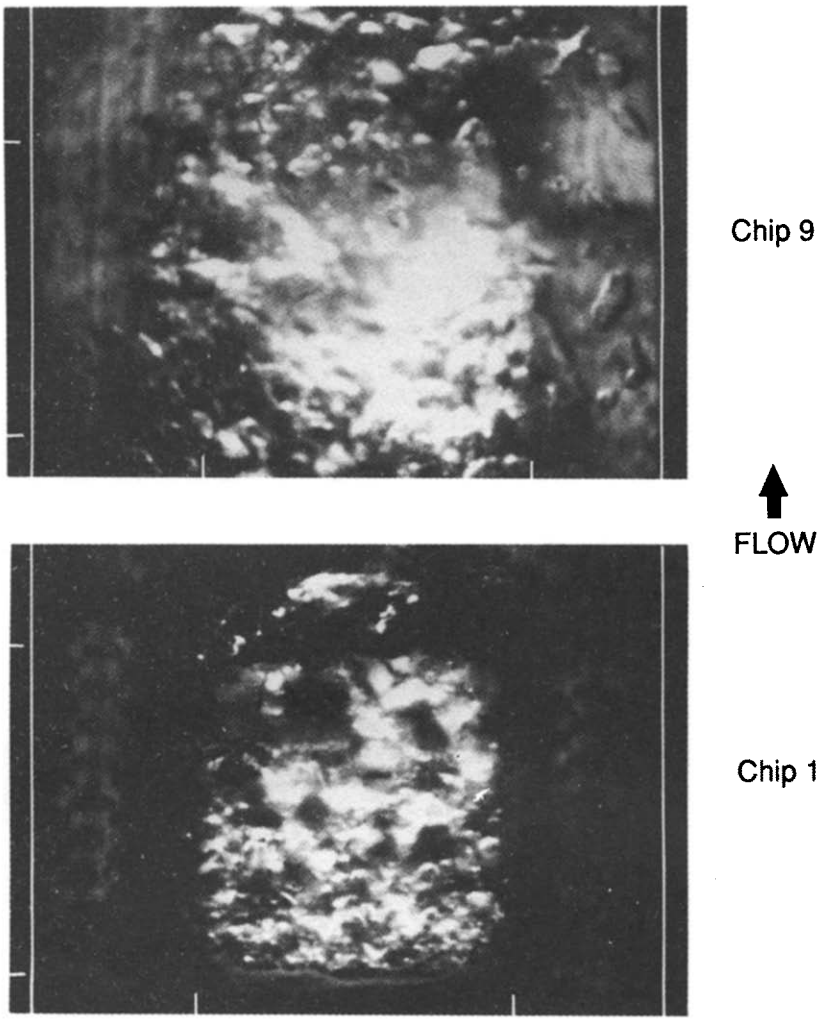

FIG. 6(b).

toward the side walls; nevertheless, bubbles were primarily concentrated in an area directly above the chips. Also, bubbles reached the top wall of the channel well upstream of Chip 9, and this produced some deformation of the bubbles against the top wall. In the 2 mm channel, the bubbles spanned the entire width of the channel and were visibly smeared against the top wall, spurring large degrees of bubble deformation and coalescence. The void fraction in the smallest channel seemed much larger than that in the other two.

Figure 7(a) is a photograph of Chip 9 in the 2 mm channel for flow at 12°C subcooling and 25 cm s^{-1} and a chip heat flux of 20 W cm^{-2}. Comparing Fig. 7(a) with Chip 9 in Fig. 6(c) reveals that increasing the subcooling significantly reduced bubble migration toward the side wall, though the void in the flow area just above the chips remained substantial at 12°C subcooling. Visibly, one can see the large degree of bubble coalescence and deformation against the top wall spawned by the small channel height. Figure 7(b) shows that increasing the velocity to 250 cm s^{-1} allowed the heat flux to be considerably increased (33 W cm^{-2}) and still fostered a reduction in the width of the bubble layer as well as a decrease in the size of individual bubbles.

Void fraction in subcooled boiling

It is possible to quantify the amount of void within the channel by using a subcooled boiling analysis that

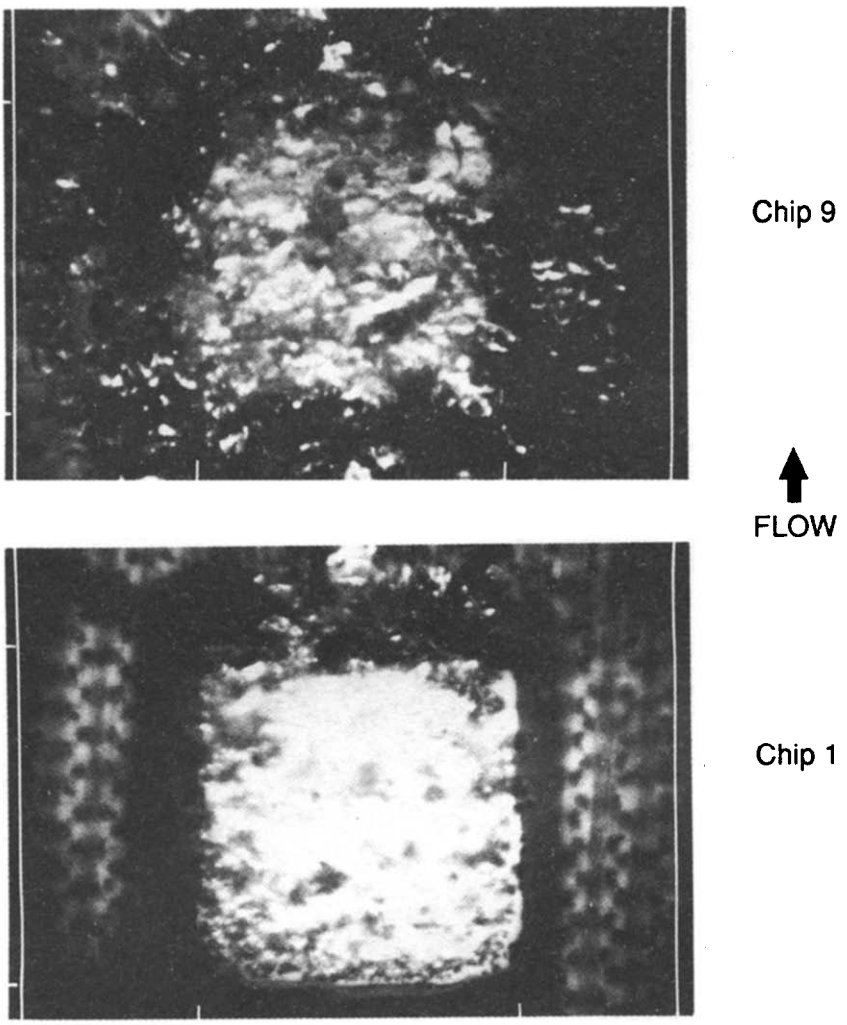

FIG. 6(c).

incorporates the drift-flux model. The flow can be idealized as subcooled liquid entering the rectangular channel, as shown in Fig. 8. A uniform heat flux is applied to one wall of the channel while the opposite wall is adiabatic. Other issues related to the discontinuity in wall heat flux and concentration of heat flux on a fraction of the heated wall will be discussed later. Initially, heat is transferred from the heated wall to the subcooled liquid by single-phase forced convection, and this produces a stream-wise increase in liquid temperature, with the near-wall temperature rising more rapidly than that of the bulk liquid. After some distance z_0 from the inlet, the near-wall liquid satisfies the superheat requirements to initiate boiling, and vapor bubbles form at the heated surface. This region of heat transfer is referred to as subcooled boiling since the temperature of the bulk liquid is still below saturation. Typically, the inability to accurately predict the point of net vapor generation is responsible for much error in the prediction of void fraction in subcooled boiling; however, the application of boiling on chips is well suited for such an analysis since, as observed experimentally and at heat fluxes of practical interest, the point of net vapor generation is always known to correspond with the upstream edge of Chip 1 (the most upstream chip). The stream-wise increase in bulk temperature continues until the temperature reaches saturation, after which the flow experiences saturated boiling until either the channel exit or eventual dryout is attained.

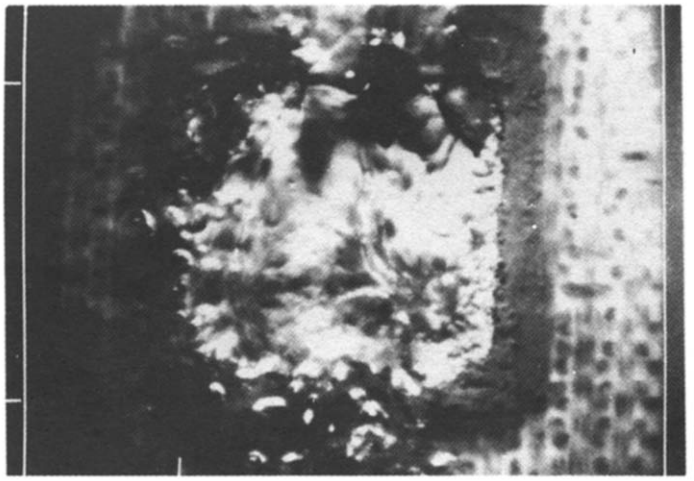

(a)

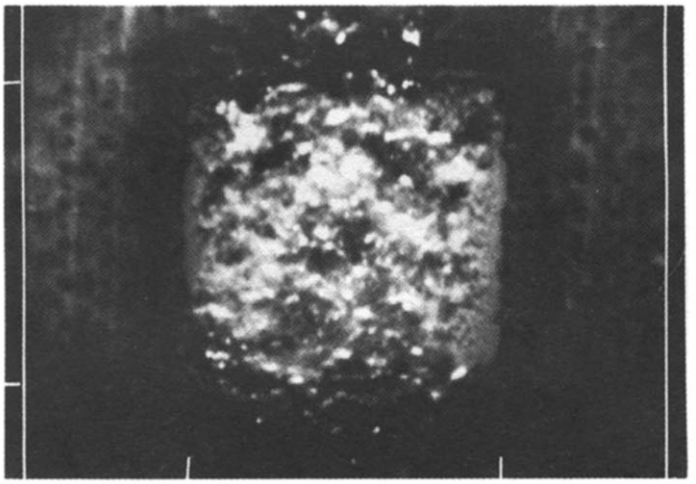

(b)

FIG. 7. Photographs of Chip 9 in the 2 mm channel for 12°C subcooled flow and velocity and heat flux of 25 cm s^{-1} and 20 W cm^{-2} (a), and 250 cm s^{-1} and 33 W cm^{-2} (b).

In order to characterize the region of subcooled boiling, it is first necessary to define the mass flow rate and vapor quality of the two-phase mixture. Since the flow is entirely subcooled liquid just upstream of z_0, mass conservation gives

$$W = \rho_f UA = W_f + W_g. \tag{1}$$

The mass vapor quality can then be defined as

$$x = \frac{W_g}{\rho_f UA}. \tag{2}$$

For thermodynamic equilibrium to be attained at z_e, a simple energy balance of the flow requires

$$q'' P_h (z_e - z_0) = \rho_f UA c_{pf} (T_{sat} - T_{f0}). \tag{3}$$

Rearranging equation (3) gives

$$z_e - z_0 = \left[\frac{\rho_f UA h_{fg}}{q'' P_h}\right]\left[\frac{c_{pf}\Delta T_{sub}}{h_{fg}}\right] \tag{4}$$

where $\Delta T_{sub} \equiv T_{sat} - T_{f0}$.

For some distance (z) inside the subcooled boiling region thermodynamic equilibrium is not satisfied, and an energy balance on the two-phase mixture yields

$$q'' P_h (z - z_0) = W_f c_{pf} (T_f(z) - T_{f0}) + W_g [c_{pf}\Delta T_{sub} + h_{fg}]. \tag{5}$$

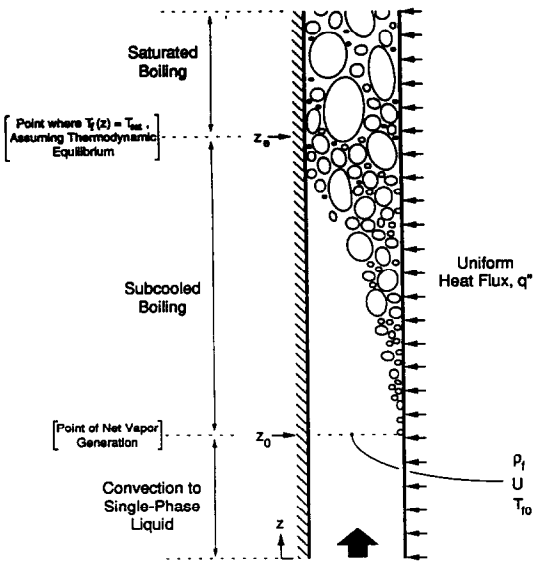

FIG. 8. Subcooled boiling in a rectangular channel.

Rearranging and substituting from equations (1) and (2) gives

$$x = \frac{\dfrac{z-z_0}{\left[\dfrac{\rho_f U A h_{fg}}{q'' P_h}\right]} - \dfrac{c_{pf}\Delta T_{sub}}{h_{fg}}\left[\dfrac{T_f(z)-T_{f0}}{\Delta T_{sub}}\right]}{1+\dfrac{c_{pf}\Delta T_{sub}}{h_{fg}}\left[1-\dfrac{T_f(z)-T_{f0}}{\Delta T_{sub}}\right]}. \quad (6)$$

In addition, Kroeger and Zuber [16] have recommended using the following relation for bulk liquid temperature:

$$T^+ \equiv \frac{T_f(z)-T_{f0}}{\Delta T_{sub}} = \tanh(Z^+) \quad (7)$$

where

$$Z^+ \equiv \frac{z-z_0}{z_e-z_0}. \quad (8)$$

Substituting equations (4), (7), and (8) into equation (6) gives

$$x = \frac{\dfrac{c_{pf}\Delta T_{sub}}{h_{fg}}[Z^+ - T^+]}{1+\dfrac{c_{pf}\Delta T_{sub}}{h_{fg}}[1-T^+]} \quad (9)$$

Thermodynamic equilibrium is satisfied at $z = z_e$; however, transition to saturated boiling occurs downstream of z_e. For saturated boiling, the thermodynamic equilibrium mass vapor quality can be calculated as

$$x_e = \frac{q'' P_h}{\rho_f U A h_{fg}}(z-z_e). \quad (10)$$

According to Collier [17], there is essentially no physical difference between subcooled and saturated boiling, and no discontinuity exists in any characterizing parameter at $z = z_e$ where $x_e = 0$. Therefore, in order to avoid discontinuity in calculating x, equation (9) should be employed even within the saturated boiling region until equations (9) and (10) render the same value, after which equation (10) should be used. It should be noted that, for the present study, equation (9) was sufficient to calculate x in all instances.

With the mass vapor quality determined, the drift-flux model [16] can be used to define the average void fraction as

$$\langle\alpha\rangle = \frac{x}{C_0\left(\dfrac{\rho_f-\rho_g}{\rho_f}\right)x + \dfrac{\rho_g}{\rho_f}\left(C_0+\dfrac{\overline{u_{gj}}}{U}\right)}. \quad (11)$$

In the drift-flux model, the relative velocity between vapor bubbles and liquid is accounted for by means of the vapor drift velocity $\overline{u_{gj}}$ defined as the vapor velocity relative to the velocity of the center of volume of the mixture. For the bubbly-churn flow regime, Zuber *et al.* [18] have suggested the weighted mean drift velocity be determined as

$$\overline{u_{gj}} = 1.41\left[\frac{\sigma g(\rho_f-\rho_g)}{\rho_f^2}\right]^{1/4}. \quad (12)$$

The distribution parameter C_0 in equation (11) is a measure of how the void and flow profiles across the channel affect the average void fraction. The value of C_0 is equal to unity for flat profiles. When the two profiles are similar and achieve peak values at the same point, C_0 can reach a maximum of 1.5; on the other hand, C_0 can decrease below unity when the peak points for the two profiles become more remote. In subcooled boiling, C_0 is approximately zero at the point of net vapor generation, and C_0 is less than unity just after z_0 where bubbles are primarily concentrated at the wall. Furthermore, the value of C_0 exceeds unity as bubbles become more concentrated in the core toward the saturated boiling region. In the absence of experimental data on void and flow profiles in the subcooled boiling region, Kroeger and Zuber [16] showed that the best predictions of the average void fraction were realized by assigning to C_0 a constant value that corresponds to the saturated boiling region. For vertically upward flow in rectangular channels, they suggested using a value of 1.4.

Predicting void fractions in the present cooling configuration was complicated by the discreteness of the wall heat flux in the axial direction. In accounting for this, the void profile was assumed to be preserved (i.e. negligible collapse of bubbles) between adjacent chips; this assumption is an upper limit in predicting void fractions for electronic cooling design purposes and is not recommended for predictions in highly subcooled flow. Void fraction determination was also complicated by the confinement of heating to a fraction of the wetted perimeter, and this created some uncertainty in selecting the appropriate flow area (A) to be used in calculations for near-saturated and low-

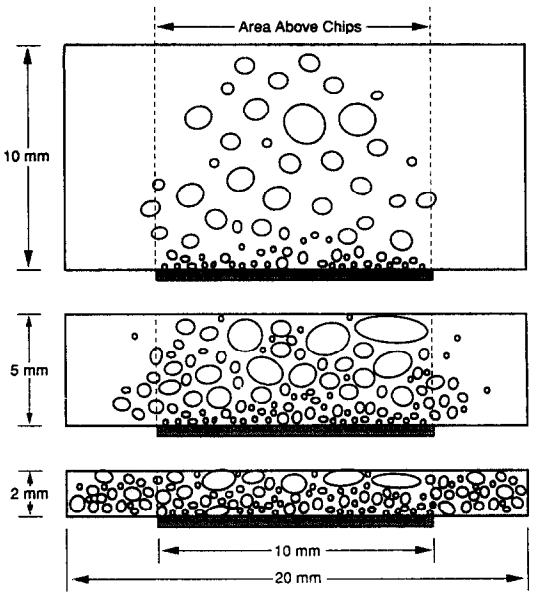

FIG. 9. Bubble population in all three channels for near-saturated flow.

subcooled flow. Figure 9 illustrates the bubble population in each channel for near-saturated flow. For the 5 and 10 mm channels, A was set equal to only the area in the channel that is directly above the chips, since flow visualization showed bubbles were primarily concentrated in this area. The true nature of interaction between the bubble layer and liquid near the side walls will be addressed later. In the 2 mm channel, bubbles in near-saturated flow consumed the entire channel and, thus, A was set equal to the entire flow area. With increases in subcooling and, to a lesser degree, increases in velocity, bubble migration in the 2 mm channel was substantially reduced such that only the area above the chips would be an appropriate choice for determining the void fraction for those conditions.

For near-saturated flow at 50 cm s^{-1} and heat flux of 17 W cm^{-2} (90% of the average value of CHF in the 2 mm channel), Fig. 10(a) illustrates the void fractions in each channel. With A equal to just the flow area directly above the chips, the analysis predicted void fractions of 62, 36, and 10% for the 2, 5, and 10 mm channels, respectively, at the downstream edge of Chip 9. Choosing the entire channel for A rather than just the area above the chips would be more consistent with visual observations for the 2 mm channel; subsequently, based upon the entire area the analysis predicted a void fraction of 45%. It is interesting to note that despite the two-fold increase in effective flow area, the 2 mm channel was still estimated to have a substantial void fraction. Figure 10(a) (and 10(b)) also highlights void fractions of 0.30 and 0.524, critical values associated with transition to slug-churn flow. Exceeding a void fraction of 0.30 drastically increases the frequency of collision between bubbles, promoting bubble coalescence and transition to slug flow [17]. A void fraction of 0.524 is the geometric value corresponding to closely packed vapor spheres; void fractions greater than 0.524 preclude the existence of bubbly flow.

At 25°C subcooling and 50 cm s^{-1}, Fig. 10(b) shows that the void fractions in the three channels just prior to CHF (30 W cm^{-2}) were 41, 6, and 0.8% when based upon just the area above the chips; based upon the entire area, a void fraction of 11% was predicted for the 2 mm channel. Flow visualization indicates that the appropriate effective area to be used in analyzing the 2 mm channel lies somewhere between the entire area and the area above the chips. Therefore, the amount of vapor in the 5 and 10 mm channels was greatly reduced with increased subcooling, but the 2 mm channel possessed a significant void fraction even at larger subcoolings. The large void fractions in the smallest channel had an impending effect on CHF values, as will be discussed later.

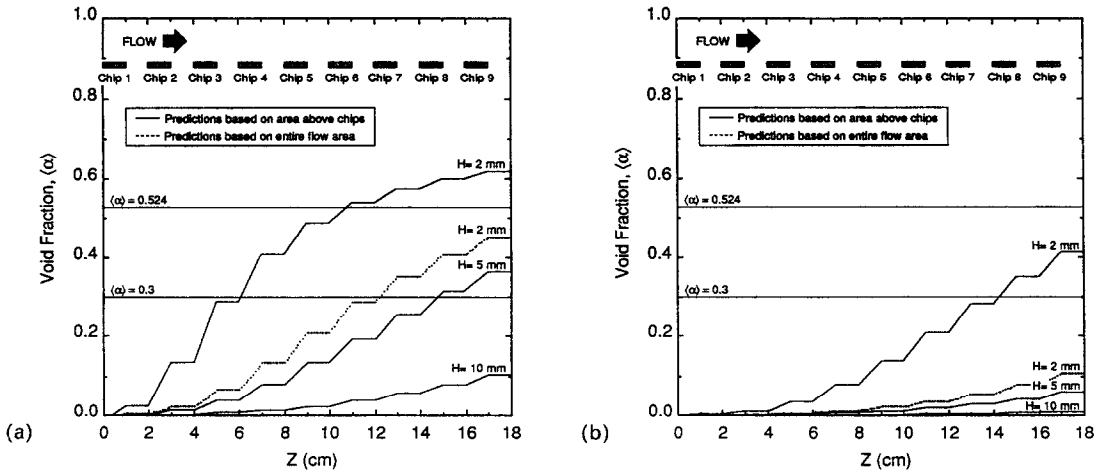

FIG. 10. Void fractions in all three channels just prior to CHF for flow at 50 cm s^{-1} and 3°C subcooling (a) and 25°C subcooling (b).

Critical heat flux

Data collection for a given experiment continued until each of the nine chips had reached CHF. Critical heat flux data at 3 and 25°C subcooling for Chips 1, 4, and 9 are shown in Figs. 11(a), (b), and (c), respectively. For all channel heights, increasing the velocity and/or subcooling generally produced an increase in CHF for the multi-chip array. Also, increases in subcooling had an even more pronounced effect on CHF at larger velocities, similar to the transition from low- to high-velocity CHF observed by Mudawar and Maddox [8] for an isolated chip. In general, the CHF values for the 5 mm channel were larger than those for the other two channels at the corresponding conditions. To illustrate the proximity of 2 and 10 mm CHF data to the 5 mm data, Fig. 11 shows a 10% band around the 5 mm data. Differences between the 5 mm data and data for the 2 and 10 mm channels were larger for Chip 1 than for either Chip 4 or Chip 9. Figure 11(a) shows that Chip 1 data for the 2 and 10 mm channels were similar, but Figs. 11(b) and (c) show that Chip 4 and Chip 9 data for the 10 mm channel were slightly larger than the corresponding data for the 2 mm channel.

As previously described, other researchers found that forced-convection CHF in narrow annuli significantly decreased when the gap spacing was reduced below a critical dimension. Similarly, in the present study CHF data for the 2 mm channel were consistently lower than the 5 mm data. Lower CHF data were also observed for a channel height much larger than the critical dimension, as evidenced by the decrease in CHF corresponding to an increase in channel height from 5 to 10 mm. Together, these two trends infer that there exists an optimal channel height for which forced-convection CHF in the rectangular channel is a maximum and, subsequently, CHF decreases as the channel height is either increased above or decreased below this optimum. These trends are well illustrated in Fig. 12, a plot of Chip 9 CHF values versus channel height for several velocities at 3 and 25°C subcooling. A second-order polynomial fit to each set of data further supports the existence of an optimal channel height, perhaps just larger than 5 mm. Also, it seems that the amount by which the maximum CHF value exceeded the data for heights of 2 and 10 mm increased with velocity and increased subcooling.

In understanding the reasons why there exists an optimal channel height for which forced-convection CHF in the rectangular channel is a maximum, it is necessary to realize that boiling trends are sensitive to channel height for a variety of mechanisms; in other words, the relationship between CHF and channel height is not monotonic, nor is it as simplistic as indicated in the literature. Furthermore, the concentration of heat flux on a portion of the heated wall adds to the complexity of explaining CHF trends, thus precluding any direct conclusions from boiling trends associated with uniformly heated walls. With these

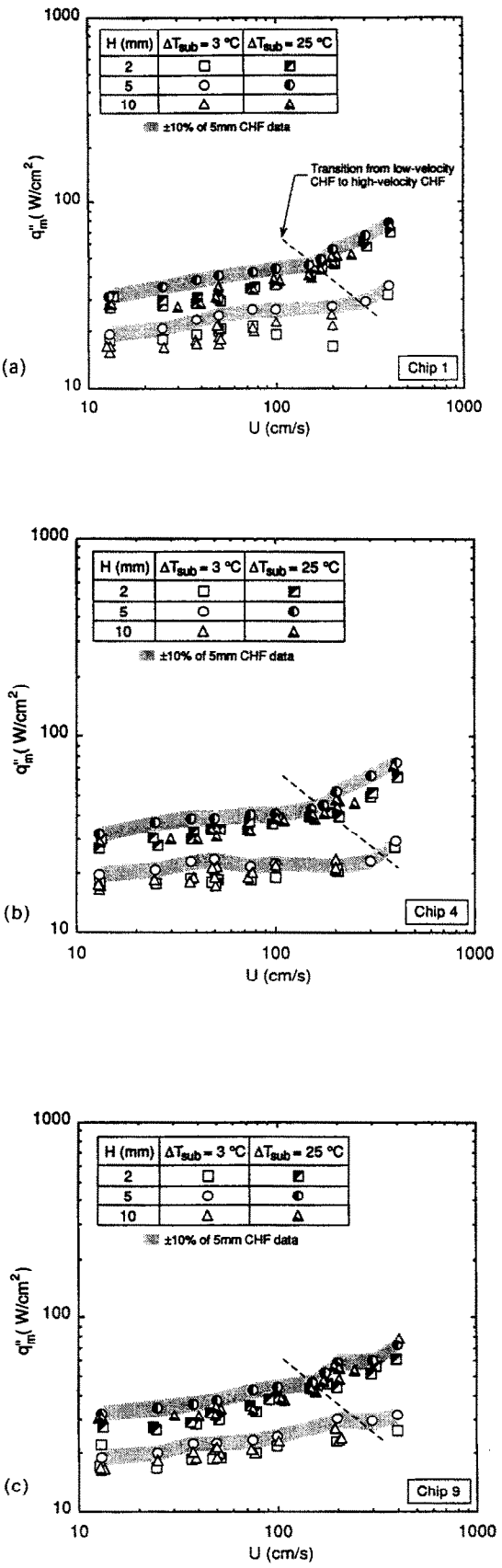

FIG. 11. Critical heat flux values at 3 and 25°C subcooling for Chip 1 (a), Chip 4 (b), and Chip 9 (c).

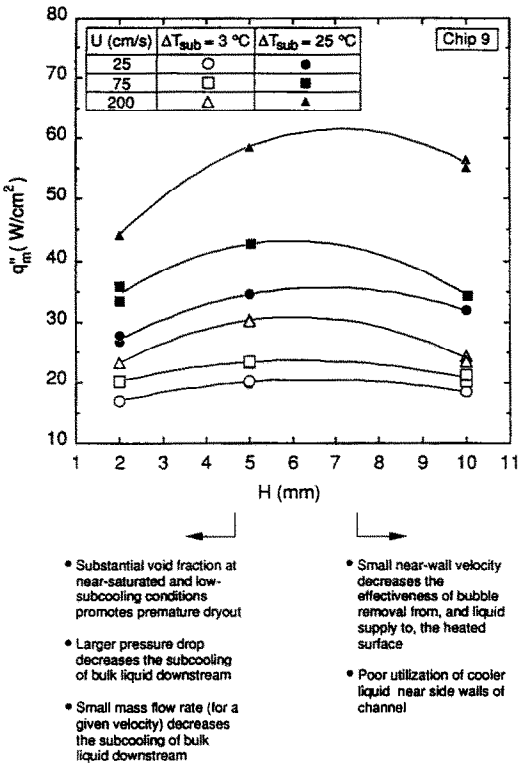

FIG. 12. Optimal channel height for which CHF is maximum.

points in mind, the existence of an optimal channel height has been explicated based upon visual observations, void predictions, and experimental data.

Both flow visualization and void fraction predictions have shown that there is a substantial amount of vapor in the 2 mm channel for flow at near-saturated and low-subcooling conditions. It can be expected that such large void fractions would stimulate premature dryout of the chip surface, thus producing lower CHF values in the 2 mm channel than those in the other channels. Premature dryout would especially be imminent for downstream chips since the void fraction increases in the flow direction. For this reason, Chip 9 CHF data for the 2 mm channel were consistently lower than Chip 9 CHF data for the 5 and 10 mm channels (Fig. 11(c)). Also, for the same reason downstream chips in the smallest channel were never the last to reach CHF for experiments at 3 and 14°C subcooling.

The substantial void fractions in the 2 mm channel were reduced with increasing velocity and subcooling due to an enhancement of bubble collapse and condensation in the bulk liquid. Nevertheless, increasing the velocity in the smallest channel engendered pressure drops across the multi-chip array that were much larger than those produced in the bigger channels, and corresponding to this reduction in pressure, there was a significant stream-wise decrease in saturation pressure (Fig. 4). Also, for a given velocity in all three channels, the smaller flow area for the 2 mm channel produced a smaller mass flow rate which, in turn, spurred a larger increase in fluid temperature for a given heat flux. The net result of decreasing saturation temperature and increasing fluid temperature in the 2 mm channel was a greater stream-wise reduction in liquid subcooling than that for the other channels. The effect of the consequential stream-wise drop in liquid subcooling is shown in Fig. 12 in that the Chip 9 CHF data in the 2 mm channel fell increasingly short of the Chip 9 CHF data in the 5 mm channel with increases in velocity and inlet subcooling.

Visual observations of the small void fraction in the 10 mm channel indicated little (if any) interaction between the heated fluid/bubbles above the chips and the cooler bulk liquid near the side walls. On the other hand, the 5 mm channel height was small enough to stimulate some bubble migration toward the side walls, but it was not so small that premature dryout was imminent as it was in the 2 mm channel. It is postulated that the subtle bubble migration and agitation in the 5 mm channel encouraged some of the cooler liquid from near the side walls to help replenish the evaporating liquid at the heated surface; however, in the 10 mm channel, rewetting of the heated surface appears to have been accomplished exclusively by the heated fluid in the thermal boundary layer above the chips. Warmer liquid would provide less sensible energy exchange at the chip surface, thus promoting early CHF; for this reason, CHF in the 10 mm channel was exceeded by that obtained in the 5 mm channel.

In addition, a close look at the idealized velocity profiles for single-phase liquid flow in all three channels reveals that, for a given mean velocity, flow in the 10 mm channel would possess a smaller stream-wise velocity at a given distance from the heated wall (i.e. reduced wall shear) than flow in the smaller channels. A smaller near-wall velocity would decrease the rate at which bubbles are swept away from, and bulk liquid supplied to, the heated surface, thus leading to a decrease in CHF.

4. CONCLUSIONS

An experimental investigation of the effects of channel height on forced-convection boiling and CHF from a linear array of discrete heat sources was conducted. Unique to these experiments was the concentration of heat flux on a fraction of the channel perimeter corresponding to the width of the heat source. The following conclusions can be drawn.

(1) Regardless of channel height, Chip 9 was generally the first to experience nucleate boiling followed by upstream chips in fairly monotonic succession. Temperature drops associated with incipience of nucleate boiling were generally larger for the 2 mm channel compared with the 5 and 10 mm channels, but there appeared to be no effect of channel height

on the fully developed nucleate boiling convection coefficient.

(2) Flow visualization in the 2 mm channel revealed that bubbles in near-saturated flow spanned the entire width of the channel, and increases in subcooling and, to a lesser degree, increases in velocity reduced the lateral spread of the bubble layer. On the other hand, bubbles in the 5 and 10 mm channels were primarily confined to an area just above the chips. These observations were confirmed by a drift-flux model of non-equilibrium subcooled flow in the channel.

(3) Experimental data, supported by void fraction predictions and flow visualization, suggest the existence of an optimal channel height for which CHF in the rectangular channel is a maximum. For equal flow velocities, maximum CHF values in the present study were obtained with the 5 mm channel. The optimal channel height was found to be the result of a variety of mechanisms which are detailed below.

The smaller channel height produced the following detrimental effects of CHF:

(a) substantial increase in void fraction at near-saturated and low-subcooling conditions;

(b) large decrease in the subcooling of the bulk liquid caused by the increased pressure drop; and

(c) large decrease in the subcooling of the bulk liquid caused by the reduced mass flow rate (for a given velocity).

The larger channel, on the other hand, resulted in the following detrimental effects on CHF:

(a) decrease in the effectiveness of bubble removal from, and liquid supply to, the heated surface caused by the decreased near-wall velocity; and

(b) poor utilization of cooler liquid near the side walls of the channel.

Acknowledgements—Support of this work by a grant from the Industrial Chemical Products Division of 3M is gratefully acknowledged. The authors also thank Mr James Githens and Mr Douglas Maddox of 3M for their technical assistance.

REFERENCES

1. R. C. Chu, Heat transfer in electronic systems, *Proc. 8th Int. Heat Transfer Conf.*, Vol. 1, pp. 293–305. San Francisco, CA (1986).
2. G. C. Vliet and G. Leppert, Critical heat flux for nearly saturated water flowing normal to a cylinder, *J. Heat Transfer* **86,** 59–67 (1964).
3. G. C. Vliet and G. Leppert, Critical heat flux for subcooled water flowing normal to a cylinder, *J. Heat Transfer* **86,** 68–74 (1964).
4. R. F. Gaertner, Photographic study of nucleate pool boiling on a horizontal surface, *J. Heat Transfer* **87,** 17–27 (1965).
5. I. Mudawar, T. A. Incropera and F. P. Incropera, Boiling heat transfer and critical heat flux in liquid films falling on vertically-mounted heat sources, *Int. J. Heat Mass Transfer* **30,** 2083–2095 (1987).
6. F. C. Gunther, Photographic study of surface-boiling heat transfer to water with forced convection, *Trans. ASME*, Ser. C, *J. Heat Transfer* **73,** 115–123 (1951).
7. S. Yilmaz and J. W. Westwater, Effect of velocity on heat transfer to boiling Freon-113, *J. Heat Transfer* **102,** 26–31 (1980).
8. I. Mudawar and D. E. Maddox, Critical heat flux in subcooled flow boiling of fluorocarbon liquid on a simulated electronic chip in a vertical rectangular channel, *Int. J. Heat Mass Transfer* **32,** 379–394 (1989).
9. B. D. Stron, V. P. Carey and W. R. McGillis, An experimental investigation of the critical heat flux conditions for subcooled convective boiling from an array of simulated microelectronic devices. In *Heat Transfer in Electronics 1989* (Edited by R. K. Shah), ASME HTD Vol. 111, pp. 135–142 (1989).
10. W. R. Gambill, Generalized prediction of burnout heat flux for flowing, subcooled, wetting liquids, *Chem. Engng Prog. Symp. Ser.* **59,** 71–83 (1963).
11. V. I. Tolubinskiy, A. K. Litoshenko and V. L. Shevtsov, Critical heat flux densities in internally-heated annuli, *Heat Transfer—Sov. Res.* **2,** 183–186 (1970).
12. Y. H. Hung and S. C. Yao, Critical heat flux of convective Freon-113 in very narrow annuli, ASME Paper 83-HT-10 (1983).
13. V. I. Tolubinskiy, A. K. Litoshenko and V. L. Shevtsov, Correlation of experimental data on critical heat fluxes in annular channels, *Heat Transfer—Sov. Res.* **1,** 80–87 (1969).
14. A. P. Ornatskiy, The effect of basic regime parameters and channel geometry on critical heat fluxes in forced convection of subcooled water, *Heat Transfer—Sov. Res.* **1,** 17–22 (1969).
15. L. S. Tong, Boiling crisis and critical heat flux, TID-25887, U.S. Atomic Energy Commission, Oak Ridge, TN, p. 26 (1972).
16. P. G. Kroeger and N. Zuber, An analysis of the effects of various parameters on the average void fractions in subcooled boiling, *Int. J. Heat Mass Transfer* **11,** 211–233 (1968).
17. J. G. Collier, *Convective Boiling and Condensation*, 2nd Edn. McGraw-Hill, New York (1972).
18. N. Zuber, F. W. Staub, G. Bijwaard and P. G. Kroeger, Steady state and transient void fraction in two-phase flow systems, General Electric Co., San Jose, CA, Report No. GEAP 5417 (1967).

EFFET DE LA HAUTEUR DU CANAL SUR L'EBULLITION EN CONVECTION FORCEE ET SUR LE FLUX CRITIQUE A PARTIR D'UN ARRANGEMENT LINEAIRE DE SOURCES DISCRETES DE CHALEUR

Résumé—Pour combler un manque de connaissance sur l'effet de la hauteur du canal sur l'ébullition en convection forcée et sur le flux critique (CHF) dans des canaux rectangulaires, des expériences sont conduites avec du FC-72 à 1,36 bar et des hauteurs de canal de 2, 5 et 10 mm. Le transfert thermique par ébullition à partir d'un arrangement linéaire de neuf sources discrètes de chaleur, simulent des puces électroniques, est étudié pour des vitesses allant de 13 à 400 cm s^{-1} et des sous-refroidissements compris entre 3 et 36°C. Une visualisation de l'écoulement proche de la saturation se répartissent dans toute la largeur du canal et que l'accroissement de la vitesse et/ou la réduction du sous-refroidissement réduit l'étalement latéral de la couche be bulles; d'autre part, des bulles dans les canaux de 5 et 10 mm sont principalement confinées à la surface juste au dessus des puces. Utilisant un modèle, on développe une analyse pour déterminer le taux de vide dans l'ébullition sous-refroidie. Les données expérimentales et les calculs suggèrent l'existence d'une hauteur optimale du canal pour laquelle le flux critique CHF est maximal. Pour des vitesses de débit égal, le CHF maximal est obtenu avec un canal de 5 mm.

EINFLUSS DER KANALHÖHE AUF DAS STRÖMUNGSSIEDEN UND DIE KRITISCHE WÄRMESTROMDICHTE AN EINER LINEAREN ANORDNUNG DISKRETER WÄRMEQUELLEN

Zusammenfassung—Der Einfluß der Kanalhöhe auf das Strömungssieden und die kritische Wärmestromdichte in rechteckigen Kanälen wurde bisher unzureichend in der Literatur beschrieben. Dies war der Anlaß für Versuche mit FC-72 bei 1,36 bar und Kanalhöhen von 2, 5 und 10 mm. An einer linearen Anordnung von 9 diskreten Wärmequellen, die Mikroelektronik-Chips darstellen, wurde der Wärmeübergang beim Sieden untersucht. Die Strömungsgeschwindigkeit wurde zwischen 13 und 400 cm je Sekunde und die Unterkühlung der Flüssigkeit zwischen 3 und 36°C variiert. Das Besondere bei den durchgeführten Versuchen war die Konzentration der Wärmestromdichte auf einen Teil des Kanalumfangs entsprechend der Breite des Chips, während auf dessen anderen Seiten das Fluid nicht beheizt wird. Im Kanal mit 2 mm Höhe zeigte sich, daß die Blasen sich bei nahezu gesättigter Strömung auf die ganze Kanalbreite verteilen. Eine Erhöhung der Geschwindigkeit und/oder der Unterkühlung verringert die seitliche Ausbreitung der Blasenschicht. In den Kanälen mit 5 und 10 mm waren die Blasen hauptsächlich auf das Gebiet über den Chips begrenzt. Unter Verwendung des Drift-Flux-Modells wurde ein Verfahren zur Bestimmung des Dampfgehalts beim unterkühlten Sieden entwickelt. Die Versuchsergebnisse weisen zusammen mit dem berechneten Dampfgehalt und den Strömungsbeobachtungen auf die Existenz einer optimalen Kanalhöhe hin, für die die kritische Wärmestromdichte ein Maximum erreicht. In der vorliegenden Arbeit wurde für konstante Geschwindigkeit bei 5 mm Kanalhöhe die maximale Wärmestromdichte erreicht.

ВЛИЯНИЕ ВЫСОТЫ КАНАЛА НА КИПЕНИЕ ПРИ ВЫНУЖДЕННОЙ КОНВЕКЦИИ И КРИТИЧЕСКИЙ ТЕПЛОВОЙ ПОТОК ОТ ЛИНЕЙНОЙ ЦЕПОЧКИ ДИСКРЕТНЫХ ТЕПЛОВЫХ ИСТОЧНИКОВ

Аннотация—Для возполнения отсутствующих в литературе данных о влиянии высоты канала на кипение при вынужденной конвекции и критический тепловой поток (КТП) в каналах прямоугольного сечения проводились эксперименты с FC-72 при давлении 1,36 бар и высоте канала, составляющей 2, 5 и 10 мм. Исследовался теплоперенос при кипении, вызванном линейной цепочкой из девяти дискретных источников тепла, моделирующих микроэлектронные чипы, в диапазонах изменения скорости и недогрева жидкости, составляющих соответственно 13–400 см · $с^{-1}$ и 3–36 °С. В экспериментах наблюдалось специфэческое распределение теплового потока на отрезке периметра канала, соответствующем ширине чипа, при течении ненагретой жидкости по одной из сторон чипов. Визуализация течения в канале диаметром 2 мм показала, что пузырьки почти насыщенного потока располагаются по всей ширине канала и увеличение скорости и (или) недогрева приводит к уменьшению поперечного размера слоя пузырьков; с другой стороны, пузырьки в каналах диаметрами 5 и 10 мм преимущественно располагались в области непосредственно над чипами. Разработана аналитическая методика для определения объемного наросодержания при кипении в процессе недогрева. Экспериментальные данные, а также результаты расчетов объемного паросодержания и визуализации течения позволяют предположить существование оптимальной высоты канала, для которой КТП при вынужденной конвекции достигает максимального значения. При равных скоростях течения максимальные значения КТП были получены в канале диаметром 5 мм.